PCCP

ROYAL SOCIETY OF CHEMISTRY

PAPER

View Article Online
View Journal

Cite this: DOI: 10.1039/d0cp01921f

High pressure single-molecule FRET studies of the lysine riboswitch: cationic and osmolytic effects on pressure induced denaturation†

Hsuan-Lei Sung[ab] and David J. Nesbitt *[abc]

Deep sea biology is known to thrive at pressures up to ≈1 kbar, which motivates fundamental biophysical studies of biomolecules under such extreme environments. In this work, the conformational equilibrium of the lysine riboswitch has been systematically investigated by single molecule FRET (smFRET) microscopy at pressures up to 1500 bar. The lysine riboswitch preferentially unfolds with increasing pressure, which signals an increase in free volume ($\Delta V^0 > 0$) upon folding of the biopolymer. Indeed, the effective lysine binding constant increases quasi-exponentially with pressure rise, which implies a significant weakening of the riboswitch–ligand interaction in a high-pressure environment. The effects of monovalent/divalent cations and osmolytes on folding are also explored to acquire additional insights into cellular mechanisms for adapting to high pressures. For example, we find that although Mg^{2+} greatly stabilizes folding of the lysine riboswitch ($\Delta\Delta G^0 < 0$), there is negligible impact on changes in free volume ($\Delta\Delta V^0 \approx 0$) and thus any pressure induced denaturation effects. Conversely, osmolytes (commonly at high concentrations in deep sea marine species) such as the trimethylamine *N*-oxide (TMAO) significantly reduce free volumes ($\Delta\Delta V^0 < 0$) and thereby diminish pressure-induced denaturation. We speculate that, besides stabilizing RNA structure, enhanced levels of TMAO in cells might increase the dynamic range for competent riboswitch folding by suppressing the pressure-induced denaturation response. This in turn could offer biological advantage for vertical migration of deep-sea species, with impacts on food searching in a resource limited environment.

Received 9th April 2020,
Accepted 5th June 2020

DOI: 10.1039/d0cp01921f

rsc.li/pccp

I. Introduction

The effective free volume of a biomolecule can vary substantially upon folding, mainly due to changes in accessibility of hydrophilic regions and compactness of the resulting water configuration.[1–4] Consequently, the equilibrium between each conformation can be modulated by pressure, according to Gibbs free energy: $\Delta G^0 = \Delta U^0 - T\Delta S^0 + P\Delta V^0$.[5,6] Although pressure is often a relatively benign variable in biology, pressure dependence of folding is extremely important to deep sea marine species, as a result of the rapid increase of hydraulic pressure with ocean depth (≈1 bar every 10 meters). In fact, multiple organisms have been found thriving in the deep sea and some even at the bottom of the Mariana Trench,[7] where pressure at the deepest point is $P \approx 1.1$ kbar. It is thus of considerable interest to investigate not only the biophysical response of biomolecules to pressure fluctuations, but also the molecular strategies developed by deep sea organisms to accommodate extreme pressures and changes in pressure by vertical migration. As an explicit focus of this work, we combine single molecule fluorescence microscopy tools in a high pressure apparatus to explore the folding dynamics of RNA riboswitches.

As a simple test construct for such studies, riboswitches are noncoding mRNA elements that can regulate their shape and gene expression in response to the specific presence of small molecular ligands.[8–11] The aptamer domain of a riboswitch structurally changes to selectively capture a specific ligand molecule(s), with which the gene expression platform may toggle between "on" and "off" conformations and thus result in disparate regulatory outcomes. In order to optimize gene regulation, therefore, the folding equilibrium of a riboswitch must be delicately modulated by a multitude of external variables such as external pressure, temperature, and concentrations of monovalent/divalent cations and osmolytes. Although external pressure might seem only a relatively small perturbation, typical free volume changes associated with DNA hairpin formation with only 7–10 bp (say, $\Delta V^0 \approx 25$ mL mol^{-1}) translate into free

[a] JILA, National Institute of Standards and Technology and University of Colorado, Boulder, CO 80309, USA. E-mail: djn@jila.colorado.edu
[b] Department of Chemistry and Biochemistry, University of Colorado, Boulder, CO 80309, USA
[c] Department of Physics, University of Colorado, Boulder, CO 80309, USA

† Electronic supplementary information (ESI) available. See DOI: 10.1039/d0cp01921f

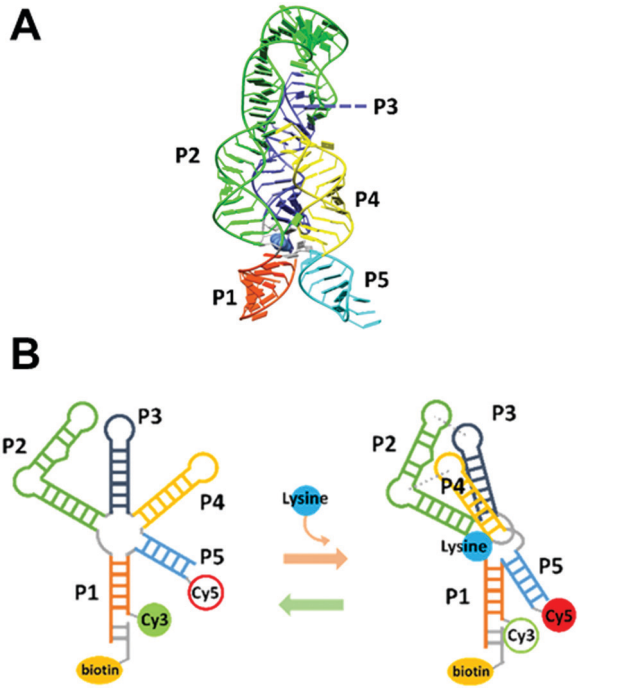

Fig. 1 Single molecule FRET construct design for studying ligand-induced lysine riboswitch folding. (A) Crystal structure of the lysine riboswitch (PDB: 4ERJ). (B) Schematic representation of lysine riboswitch folding and the energy transfer between Cy3 and Cy5 in each conformation (left: unfolded; right: folded).

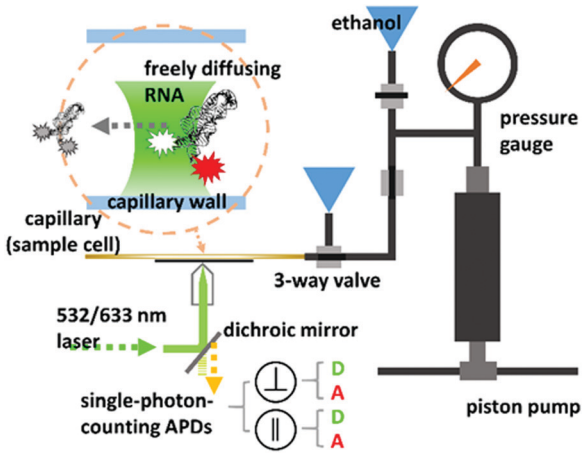

Fig. 2 High pressure smFRET diffusing experiment setup.

energy changes of $\approx$0.6 kcal mol^{-1} $\approx$ kT at 1 kbar pressures common to deep ocean marine life.[12] To date, pressure-dependent studies of nucleic acid folding have been largely limited to secondary structure formation,[12–18] with studies of higher order (tertiary) interactions only for the DNA G-quadruplex[19–21] and RNA tetraloop–tetraloop receptor (TL–TLR).[22] This leaves the highly diverse arena of RNA riboswitch tertiary structure motifs largely uninvestigated and ripe for further exploration as a function of external hydrostatic pressure. In the present work, we have chosen the lysine riboswitch[23] (see Fig. 1) as a model system to study the pressure dependent effects on ligand binding and tertiary folding, both of which are among the most important conformational transitions in biologically functional RNA.

To achieve these goals, we have recently converted our single molecule confocal FRET (smFRET) apparatus into a novel tool for biomolecular folding studies at high pressure (see Fig. 2).[12,17,18,24] The present high pressure smFRET measurements are performed in a square (50 μm × 50 μm) quartz capillary sample cell, which due to relatively small surface area of the inner capillary can sustain pressures up to 5 kbar without shattering.[12] Such a large dynamic range of pressures enables us to obtain precise measurement of free volume differences upon nucleic acid folding (ΔV^0), as well as changes in these free volumes ($\Delta\Delta V^0$) in response to various cationic and osmolytic buffer conditions.

The basic organization of this paper is as follows. Key aspects of the (i) high pressure confocal experimental apparatus, (ii) construct design and preparation, and (iii) sample data analysis are presented in Section IIA–C, followed by a detailed pressure dependent studies under a variety of buffer conditions. Specifically, since both solvent and solute, in addition to the biomolecule itself, can contribute significantly to the folding thermodynamics,[25–27] the pressure-dependent response of the lysine riboswitch has been systematically studied as a function of three classes of solutes: (i) ligand (lysine), (ii) monovalent (Na^+) and divalent (Mg^{2+}) cations, and (iii) osmolyte (trimethylamine *N*-oxide, TMAO) concentrations, as presented in Section IIIA–D. First of all, as the cognate ligand, lysine plays an obviously central role in lysine riboswitch folding, which from previous detailed kinetic analyses[28] has been shown to be triggered by a single lysine in a ''induced-fit'' mechanism, whereby the ligand first binds and then folds.[28,29] Secondly, nucleic acids interact strongly with cations, due to the polyanionic nature of the RNA polymer. Thus, cationic solute species as Na^+ and Mg^{2+} can not only result in compaction of a folded (or unfolded) nucleic acid structure, but also significantly alter the hydration shell through partial Debye shielding of the Coulomb interactions.[30,31] Thirdly, TMAO is an osmolyte commonly found in marine species,[32,33] with increasing accumulations in deep sea fish and amphipods.[34,35] Moreover, TMAO has been shown to act as a chemical chaperone[36] to stabilize protein[37,38] and nucleic acids[39,40] structures at ambient pressures, and to preserve enzyme activity at high pressures.[41,42] These suggest TMAO to be a crucial ''piezolyte'' with which to counteract pressure induced denaturation effects. Indeed, in the present work, we find that an increase in TMAO results in a novel preferential stabilization of the folded riboswitch conformation at high pressure ($\Delta\Delta V^0 < 0$), thereby counterbalancing the above-noted tendency for RNA to be destabilized with increasing pressure, as discussed further in Section IV. Finally, the paper presents summary results, possible directions for future investigation, and concluding remarks in Section V.

II. Experiment

A. High pressure capillary sample cell and pressure control

These high pressure smFRET experiments are made possible by introduction of a high pressure glass capillary sample cell[12,18,24] into a time correlated single photon counting confocal microscope

(see Fig. 2).[43] Specifically, for the sample cell we use square capillary tubing made from fused silica, with ≈360 μm and ≈50 μm outer and inner sidewall lengths, respectively (Polymicro, Phoenix, AZ). Due to the small surface area of the inner capillary, the cell can sustain repeated high internal pressure cycling up to 5 kbar without fracturing. Moreover, the wall thickness (≈155 μm) and relatively flat interior and exterior surfaces of the square capillary mimic a standard cover slip and thereby optimize the excitation/collection photon efficiencies for fluorescence studies.

To prepare a sample for high pressure smFRET study, one end of the capillary is first glued to a modified stainless-steel pressure plug (High Pressure Equipment, Erie, PA). A small section of the opaque hydrocarbon polymer coating of the capillary is then removed by low temperature propane flame oxidation to create a clear optical window for fluorescence excitation and detection. We load the sample by capillary forces, simply immersing one end into the sample solution; once the capillary is filled, its free end (far from the pressure plug) is sealed by momentary heating with an oxy-propane torch. Prior to coupling the cell to the high pressure system, the open end of the capillary is dipped into low viscosity silicone oil to create a thin, immiscible liquid layer. This prevents any contamination of the sample from the pressure-transmitting ethanol and yet still conducts pressure effectively from the hydraulic press (*vide infra*) to the single molecule detection volume. More detailed description of sample cell preparation and alignment of the excitation/fluorescence microscope can be found in our previous work.[12]

The source of high pressure is a manually operated piston screw pump (High Pressure Equipment) which can generate and deliver pressures up to 5 kilobars. The pressure generator is connected to the sample cell and a Bourdon pressure gauge *via* high pressure stainless steel tubing with 1/4″ O.D. and 1/16″ I.D. (High Pressure Equipment, rated at 100 000 psi), with the entire manifold using ethanol as the pressure-transmitting fluid. Prior to high pressure experimentation, any residual air bubbles in the manifold are removed by repeatedly venting and flushing the high pressure valves. The end-point absence of any residual air bubble is unambiguously evidenced by dramatic increase in the pressurizing efficiency with manual displacement of the piston screw pump.

B. RNA lysine riboswitch construct and sample preparation

The crystal structure of the *B. subtilis* lysC riboswitch aptamer is shown in Fig. 1A.[23] According to previous structural characterizations of the ligand-bound and ligand-free lysC aptamer domain,[23,44,45] the lysine induced conformational change (Fig. 1B) mostly likely involves a change in the relative orientation of the P1 and P5 helices in response to ligand binding at the five-way aptamer junction. Therefore, to optimize smFRET contrast in the construct design, the Cy3 and Cy5 dyes are attached at the distal ends of P1 and P5, respectively (Fig. 1B).[28] The three-strand lysine riboswitch smFRET construct is specifically illustrated in Fig. 1B, with detailed RNA oligomer designs and synthesis methods available from our previous lysine riboswitch studies under ambient pressure conditions.[28] In anticipation of future smFRET studies, we have also incorporated an additional biotin modification at the extended P1 stem for tethering the RNA construct onto BSA–biotin/streptavidin modified surfaces, which will restrict free diffusion and enable much longer observation times for studies of single molecule kinetics. For maximum simplicity in these early high-pressure experiments, however, we have chosen to not tether the construct to the surface. This allows the RNA riboswitch construct to freely diffuse in the capillary cell through the laser beam focus, for which detection/sorting fluorescence photon "bursts" ($\tau \sim 1$ ms duration) through dichroic filters onto avalanche photodiodes permit statistical probing of the instantaneous biomolecular conformations by smFRET.

In preparation for smFRET sample solutions, the stock RNA solution is diluted in imaging buffer to ~50 pM, *i.e.*, sufficiently low that each fluorescence burst results exclusively from only one doubly-labeled construct diffusing through the confocal volume. The imaging buffer contains (i) 50 mM hemipotassium HEPEs buffer (pH 7.5), (ii) Trolox/PCA/PCD oxygen scavenger cocktail to catalytically remove oxygen, (iii) 25 mM KCl, 100 mM NaCl and 0.5 mM $MgCl_2$ to provide background salt, and (iv) sufficient lysine, TMAO, additional NaCl and $MgCl_2$ to achieve the desired experimental conditions.

C. Single-molecule FRET spectroscopy and data analysis

The high pressure smFRET experiment is based on a homebuilt inverted confocal microscope setup with details described in previous work (Fig. 2).[43] In short, a water immersion objective with 1.2 NA tightly focuses the collimated incident beam into a nearly diffraction limited spot ($1/e^2$ radius = 310(30) nm). The resulting fluorescent photons are collected through the same objective, sorted into spatially distinct color/polarization channels with dichroic filters/polarization cubes before being detected by an array of four single-photon counting avalanche photodiodes. Since the double fluorophore labelling efficiency is <100%, alternating laser excitation methods (ALEX) with interleaving green and red laser pulses are used to rigorously ensure that only bursts from doubly-labeled RNA constructs are included in the FRET energy transfer efficiency (E_{FRET}) distributions.[28,46] Sample fluorescence traces are exhibited in Fig. 3A and B, with the ALEX signal plotted downward (pink) to distinguish it from the upward FRET (green/red) emission channels. By way of example, the series of photon events flagged by arrows in Fig. 3B and numbered from 1 to 3 can be unambiguously sorted into fluorescent bursts corresponding to (1) doubly labeled, (2) Cy3 only and (3) Cy5 only RNA constructs, respectively.

Integrated over the full burst diffusion time, the E_{FRET} value ($E_{FRET} = I_A/(I_A + I_D)$) for each event from doubly-labeled DNA is computed and used to generate a E_{FRET} histogram (Fig. 3C). The lysine riboswitch histogram clearly reveals two distinct populations with low E_{FRET} (~0.3) and high E_{FRET} (~0.7) states, which corresponds well with predictions for unfolded and folded conformations, respectively.[28] Therefore, data are fit to a two-Gaussian distribution function with the center and width of the high E_{FRET} peak floating globally (Fig. 3C).[28,46] As a function of hydrostatic external pressure, the unfolded population clearly

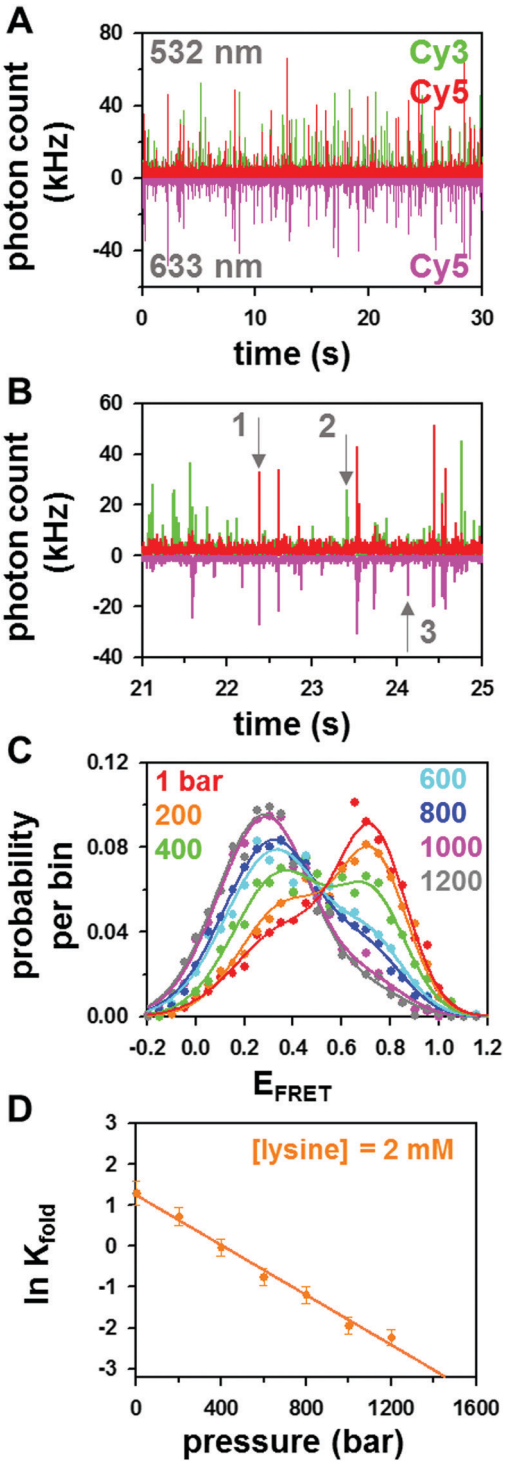

Fig. 3 Sample data and analysis. (A) Representative time-resolved fluorescence trajectories. The green and red signals plotted upward correspond to Cy3 and Cy5 fluorescence channels, respectively. The pink traces from 633 nm alternating laser excitation (ALEX) is plotted downward for direct comparison to conform the presence (or absence) of the Cy5 labeling. (B) Detailed fluorescent traces displaying individual fluorescent events: (1) folded doubly labeled, (2) Cy3-only and (3) Cy5-only labeled construct. (C) Sample E_{FRET} histogram of the lysine riboswitch folding with [lysine] = 2.0 mM at increasing pressure. Each set of data is fit to a two-Gaussian function where the high and low E_{FRET} populations correspond to folded and unfolded conformations of the lysine riboswitch respectively. (D) The $\ln(K_{fold})$ *vs.* P plot where the slope yields the free volume change during folding ΔV^0.

increases while the folded population decreases (see Fig. 3C). The relative abundance of the two states can be quantified by taking the ratio of the areas under the two fitted Gaussian functions to obtain the riboswitch equilibrium constant for folding. Note that under saturating lysine/salt concentrations, the maximum fraction of free diffusing riboswitch constructs folded is only 71(8)% of the value obtained from direct single-molecule observation of an immobilized construct (see Fig. S1, ESI†). This fraction is in good agreement with previous reported values of 67(3)% in earlier riboswitch studies restricted to a narrower range of [lysine] due to time resolution limits.[28] As shown previously, such discrepancies between the diffusing and immobilized measurements occur because a small fraction (28(4)%) of the constructs are stuck in long lived misfolded states, with only 72(4)% actively undergoing conformational transitions.[28] Thus, accurate extraction of single molecule equilibrium constants (K_{fold}) is obtained after correction for the inactive non-folding subpopulations,[47,48] with these corrected values used in all further analyses.

III. Results and analysis

A. Pressure-induced denaturation of the lysine riboswitch

The systematic decrease in the folded (high E_{FRET} state) construct population as a function of increasing pressure (Fig. 3C) clearly indicates that folding of the lysine riboswitch is energetically disfavored at high pressure. We can quantitatively express the pressure dependence of this folding equilibrium constant from[5]

$$\left(\frac{\partial \ln K_{fold}}{\partial P}\right)_T = \frac{-\Delta V^0}{RT}, \quad (1)$$

where R is the gas constant and ΔV^0 denotes the change in effective free volume upon folding: $\Delta V^0 = V_{fold} - V_{unfold}$. The pressure induced denaturation we see experimentally signifies that $\Delta V^0 > 0$, *e.g.* the effective free volume increases upon folding. Such a free volume change can be further quantified by a $\ln(K_{fold})$ *vs.* pressure "van't Hoff" plot (Fig. 3D), for which eqn (1) predicts a slope of $-\Delta V^0/RT$. In Fig. 3D, the free volume change of lysine riboswitch folding at [lysine] = 2 mM is extracted from a linear least squares fit to be $\Delta V^0 = +75(3)$ mL mol^{-1}.

The positive sign of this free volume change may seem at first counterintuitive. The folded RNA state is generally thought to be more compact in size, but such intuitions are only valid for the solute and ignore the complete solute + solvent system. The positive ΔV^0 values therefore arise from changes not just in the biopolymer solute itself but in the effective volume of the surrounding solvent and solvent accessibility.[1–4] For example, unfolded RNA presents a less shielded polyanionic conformation to the solvent, which therefore becomes more hydrated due to larger solvent-exposed surface area. This could in general result in a more highly ordered hydration shell with smaller effective volume and therefore a $\Delta V^0 > 0$ upon refolding.[10,49] Alternatively, folding with more tertiary/higher order contacts can create hydrophobic voids that exclude water molecules, which would also contribute to the folded state occupying an effectively larger volume with $\Delta V^0 > 0$.[2] We note that similarly counterintuitive

behavior also occurs in high pressure studies of protein folding, which routinely indicate pressure induced denaturation effects consistent with $\Delta V^0 > 0$.[4,5] One clear takehome message from the anomalous sign of ΔV^0 for nucleic acid and proteins is that coupled solute + solvent dynamics must play an exceedingly important synergistic role and cannot be ignored.

It is also worth noting that these $\Delta V^0 \approx 75(3)$ mL mol^{-1} free volume changes in the lysine riboswitch are an order of magnitude larger than the $\Delta V^0 \approx 5$ to 9 mL mol^{-1} values obtained from bulk fluorescence studies of the RNA tetraloop–tetraloop receptor (TL–TLR) at high pressures over a series of buffer conditions.[22] However, given that multiple tertiary structure formations are involved in lysine riboswitch folding, these differences become much easier to rationalize.[23] Indeed, the lysine riboswitch construct is a much more complex RNA folding motif than the simple TL–TLR system, with a multi-helix junction connecting 5 mutually interacting stem-loops. Moreover, the lysine riboswitch also has a larger molecular size (~6 kDa) comparable to that of a small protein. Thus, the ΔV^0 values measured for the lysine riboswitch are in fact on par with values measured for small proteins (≈50–150 mL mol^{-1}) over a similar range of molecule weights (10–20 kDa).[37,41]

B. Pressure-dependent effects on ligand-induced folding of the lysine riboswitch

Binding of the cognate ligand lysine to the 5-way junction promotes the folded state of the riboswitch and thus brings stem 1 and stem 5 in close proximity (Fig. 1B).[28] The association of a lysine molecule has been previously identified to be crucial for conformational change of the lysine riboswitch through an "induced-fit" (*i.e.*, bind-then-fold), mechanism,[28] suggesting a well-defined ligand-bound folded conformation.[29] We are therefore naturally interested in the role of ligand in promoting or decreasing the pressure stability of the well-established ligand–riboswitch interaction. The pressure dependence of lysine riboswitch folding has been studied as a function of [lysine] from 0.5 to 8 mM. Since lysine (side chain pK_a = 10.5) is already positively charged in our buffer (pH ~ 7.5), this could in principle influence the riboswitch stability due to Debye shielding effects in the Na^+ and Mg^{2+} cation studies reported below. To specifically isolate the ligand–aptamer interactions from the less ligand-specific effects due to the positive charge of lysine, the dynamic range of lysine concentrations explored has therefore been restricted to <10 mM, *i.e.*, more than an order of magnitude lower than typical [Na^+] values (>100 mM) previously shown necessary to promote nucleic acid stability.[43,50]

The pressure dependence of K_{fold} as a function of [lysine] is displayed as a logarithmic plot in Fig. 4A, with each set of data well fit to a linear function predicted by eqn (1). By visual inspection, the slopes remain relatively unaffected, while the intercepts all vertically shift upwards with increasing [lysine]. Stated alternatively, the presence of lysine significantly stabilizes the folding of the lysine riboswitch, and yet with negligible effect on any change in the free volume ($\Delta\Delta V^0 \approx 0$). The results are more quantitatively summarized in Table 1, where ΔV^0 is plotted in Fig. 4B as a function of [lysine]. Fig. 4B demonstrates

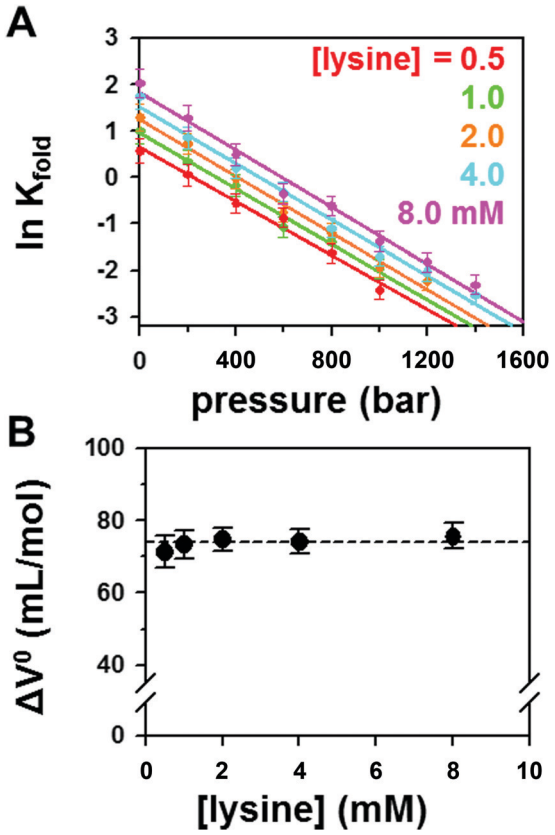

Fig. 4 Pressure dependence of folding at series of ligand (lysine) concentrations. (A) ln(K_{fold}) *vs.* *P* plot where the parallel lines indicate constant ΔV^0. (B) The insensitivity of folding ΔV^0 to lysine concentration where the error bars are visually magnified by two with the vertical break.

Table 1 ΔV^0 obtained at increasing [lysine]

[Lysine] (mM)	0.5	1.0	2.0	4.0	8.0
ΔV^0 (mL mol^{-1})	71(4)	73(3)	75(3)	74(3)	76(3)

the remarkable insensitivity of ΔV^0 to lysine concentrations (note the break in the vertical axis, visually magnifying any such lysine dependences by a factor of two).

For ligand-induced riboswitch folding, the dissociation constant is a common measure of the ligand–RNA interaction strength,[51] where K_d is equivalent to the lysine concentration at the point of 50% folding, *i.e.*, where [folded] ≈ [unfolded] and thus ln(K_{fold}) = 0. One should note that K_d represents an apparent dissociation constant, since the actual ligand binding and riboswitch folding event (which triggers the FRET change) could in principle be decoupled and separated in time.[29] Conveniently restated, we can therefore empirically determine the corresponding 50% pressures ($P_{50\%}$) for which [lysine] equals K_d from the data in Fig. 4A, obtained from the intersection of each least squares fit with ln(K_{fold}) = 0. For example, the *x*-intercept for [lysine] = 0.5 mM corresponds to $P_{50\%} \approx 221$ bar (see Fig. 4A), which implies that at 221 bar applied pressure, the lysine riboswitch is 50% unfolded and thus $K_d \approx 0.5$ mM. In this fashion, the results in Fig. 4A can be more usefully

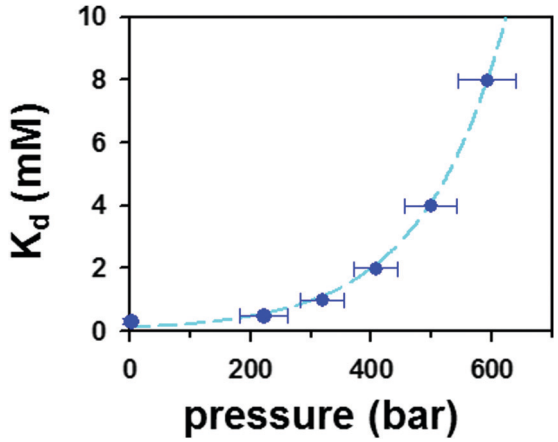

Fig. 5 Pressure effects on apparent K_d of lysine binding. K_d increases exponentially with pressures, suggesting riboswitch–ligand interactions are efficiently weakened at high pressures.

replotted as K_d *vs.* applied pressure (see Fig. 5), where we have included the value (K_d = 0.31(10) mM) determined from concentration dependent folding at ambient pressure (see Fig. S1, ESI†). Interestingly, Fig. 5 reveals that the dissociation constant K_d increases dramatically and indeed roughly exponentially as a function of increasing pressure. On the one hand, this result follows immediately from the fact that the plots in Fig. 4A are linear and free energies scale as the logarithm of equilibrium constants. On the other hand, our simple restatement of the data in terms of the apparent lysine K_d suggests a subtler interpretation – that external pressure weakens the apparent binding/binding-induced folding of lysine to the riboswitch. Furthermore, this behavior predicts that weakening of the RNA–ligand interaction becomes exponentially more significant at higher pressure. For example, at the bottom of the Mariana Trench (≈1.1 kbar), Fig. 5 predicts that K_d will be increased by 3 orders of magnitude (≈300 mM), signaling much higher [lysine] required to achieve biochemically competent folding of the riboswitch. Due to such strong denaturation influences, one anticipates the need for deep sea organisms to develop adaptive mechanisms to counteract pressure in order to maintain correct biochemical function,[32,33] a point to which we will return and discuss further in Section IVC.

C. Cation effects on pressure dependent folding of the lysine riboswitch

Nucleic acids are highly negatively charged polymers, with one phosphate group per nucleotide and which therefore interact strongly with solute cations. It has been well established that mono- and divalent cations are crucial to stabilizing the native structure of a nucleic acid riboswitch, with tertiary interactions in the riboswitch folding particularly sensitive to physiologically important multivalent cations such as Mg^{2+}.[30,31,52–55] We thus are naturally interested in both monovalent and divalent cation effects on the pressure dependent response of the lysine riboswitch. To explore the monovalent cation effects, the pressure dependence on riboswitch folding is first studied as a function of [Na^+] at constant divalent ([Mg^{2+}] = 0.5 mM) and

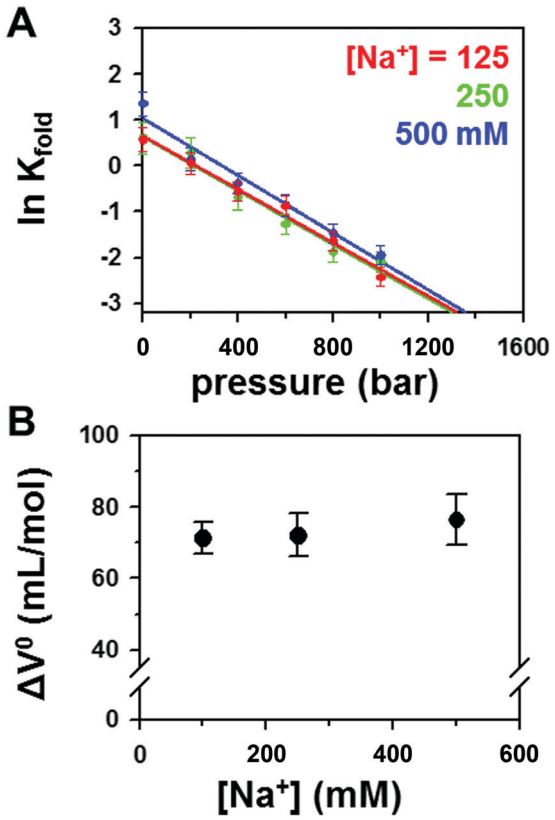

Fig. 6 Pressure dependence of folding at series of Na^+ concentrations. (A) ln(K_{fold}) *vs.* *P* plot where folding shows negligible dependence on [Na^+]. (B) [Na^+] (in)dependence of ΔV^0.

ligand ([lysine] = 0.5 mM) concentrations (Fig. 6A). Interestingly, over the physiologically relevant scale of [Na^+] from 100 to 500 mM, the effects are quite similar to that of lysine, *i.e.*, with the slopes in Fig. 6A predicting essentially negligible dependence of free volume change on Na^+. Indeed, the slopes are indistinguishable within experimental uncertainty, which from the above lysine analysis indicates that (i) ΔV^0 is independent of Na^+ over physiological range and (ii) the dependence of K_{fold} on pressure is insensitive to [Na^+] from ambient up to 1 kbar. These ΔV^0 results are quantitatively summarized in Fig. 6B and Table 2, with the data confirming that both the folding equilibrium constant and its pressure-dependent response remain relatively constant over the range of physiologically relevant [Na^+].

We next turn to the effects of divalent Mg^{2+} on this pressure dependent riboswitch folding. Once again, the slopes (see Fig. 7) in each of the plots of ln(K_{fold}) *vs.* *P* plots are equal within experimental uncertainty. This implies no Mg^{2+} dependence to free volume changes observed upon folding of the lysine riboswitch, as more quantitatively captured in the nearly horizontal data plot in Fig. 7B. This contrasts, however, with the monovalent Na^+ results in that there are very significant effects on K_{fold} due to the presence of Mg^{2+} even at ambient pressure (Fig. 7A). Note that the range of [Mg^{2+}] studied is nearly 3 orders of magnitudes lower than [Na^+], again indicating much stronger Mg^{2+} stabilization effects on RNA tertiary structures and consistent with many previous studies.[30,31,45,56] In the

Table 2 ΔV^0 obtained at increasing monovalent (Na^+)/divalent (Mg^{2+}) cation concentrations

$[Na^+]$ (mM)	125	250	500
ΔV^0 (mL mol^{-1})	71(4)	72(5)	76(6)
$[Mg^{2+}]$ (mM)	0.5	1.0	1.5
ΔV^0 (mL mol^{-1})	71(4)	69(6)	72(6)

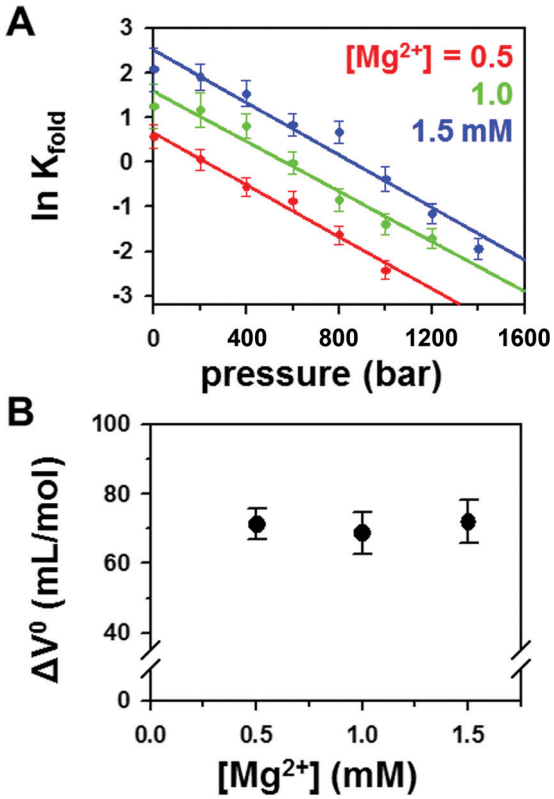

Fig. 7 Pressure dependence of folding at series of Mg^{2+} concentrations. (A) $\ln(K_{fold})$ *vs.* *P* plot where Mg^{2+} greatly promotes folding, while leaving the slopes (ΔV^0) mostly unchanged. (B) $[Mg^{2+}]$ (in)dependence of ΔV^0.

$\ln(K_{fold})$ *vs.* pressure plots in Fig. 7A, the least squares fits reveal ΔV^0 to remain nearly constant (as echoed in Fig. 7B and Table 2), while the significant upward vertical shifts in Fig. 7A indicate that Mg^{2+} strongly stabilizes the folded lysine riboswitch at all pressures. We note that the independence of ΔV^0 on Na^+ and Mg^{2+} demonstrated in Fig. 6A and 7A is quite different from previous studies, where ΔV^0 for DNA/RNA folding was found to be sensitive to cations.[22,57] For instance, ΔV^0 for folding of the 40A DNA hairpin is reduced from 11.5(35) mL mol^{-1} to 5.9(10) mL mol^{-1} with $[Mg^{2+}]$ increasing from 0.3 mM to 1.0 mM ($\Delta\Delta V^0 < 0$),[57] while the ΔV^0 of TL–TLR formation increases from 5(3) mL mol^{-1} to 9(2) mL mol^{-1} with $[Mg^{2+}]$ increasing from 0 mM to 1.0 mM ($\Delta\Delta V^0 > 0$).[22] Despite the fact that the pressure denaturation is repeatedly observed (*i.e.*, $\Delta V^0 > 0$) for each nucleic acid structure, the differential cation response ($\Delta\Delta V^0$) can change sign depending on the interactions involved in the folding. A simple framework with which to understand cation effects is by charge neutralization/association between the cations and nucleic acids, resulting in a weaker hydration structure.[58] At first this would seem to predict a reduced ΔV^0 at higher cation concentrations ($\Delta\Delta V^0 < 0$) as the hydrating water molecules become less ordered.[10,49] However, just as for nucleic acid conformations, the solvent configuration is also highly dynamic during nucleic acid folding; therefore, the additional cations may preferentially interact with either the folded/unfolded state or only stay in the bulk/hydration shell during folding. As a result, the presence of cations could give rise to negative, zero or positive values of $\Delta\Delta V^0$ simply due to the redistribution of hydration at different stages of folding.[22,57] Such cationic association along the riboswitch folding coordinate further motivates future pressure dependent analysis of the folding kinetics, which may provide additional physical insights with which to help interpret such cation response from a structural perspective.

Finally, the apparent lack of Na^+ influence on pressure dependent folding of the full lysine riboswitch is noteworthy, since monovalent cations have been shown to promote formation of the isolated TL–TLR folding motif at the hundred millimolar level.[31,59] However, multiple tertiary contacts in the *Tetrahymena thermophila* ribozyme have been shown to be unresponsive to Na^+ up to $[Na^+]$ = 1.5 M in previous X-ray footprinting studies,[56] suggesting that Mg^{2+} can be crucial to certain tertiary folding motifs such as bending at internal loops.[56,60] A similar metal ion dependence can also be observed in the hairpin ribozyme[61] and its four-way junction,[62] where from E_{FRET} differences it appears that monovalent Na^+-induced compaction only partially folds the RNA in the absence of divalent Mg^{2+}. Indeed, even simpler tertiary folding motifs (such as the RNA kink-turn) may adopt different conformations in the presence of Na^+ *vs.* Mg^{2+}.[63,64] Furthermore, the importance of Mg^{2+} in the lysine riboswitch folding can be seen in the strongly $[Mg^{2+}]$-dependent K_d for lysine binding.[28,44,45] Moreover, most of the monovalent cation effects have been studied in the absence of multivalent cations.[31] In our experiments, Na^+ must compete with 0.5 mM Mg^{2+} to interact with the lysine riboswitch and thus the results could be dominated by the more prominent Mg^{2+} effects.[65]

D. TMAO effects on the pressure dependent lysine riboswitch folding

We now return to the experimental dependence of the K_d ligand binding affinity on external pressure. Many marine organisms accumulate small organic molecules known as osmolytes inside cells to adjust cellular osmotic pressures against sea water.[35,66] Much of these osmolytes are thought to have cytoprotective roles to stabilize biomolecular structures against environmental stressors such as temperature and pressure.[67] Indeed, the TMAO contents of fish and amphipods have been recently found to correlate strongly with ocean depth, further corroborating the protective role of TMAO against hydraulic pressure.[34,35] As a final focus of this paper, we have explored the influence of TMAO osmolyte concentration on folding of the lysine riboswitch, with the hope of gaining additional molecular insight into the mechanism of TMAO stabilization on RNA tertiary folding of the lysine riboswitch and ligand binding under extreme pressures.

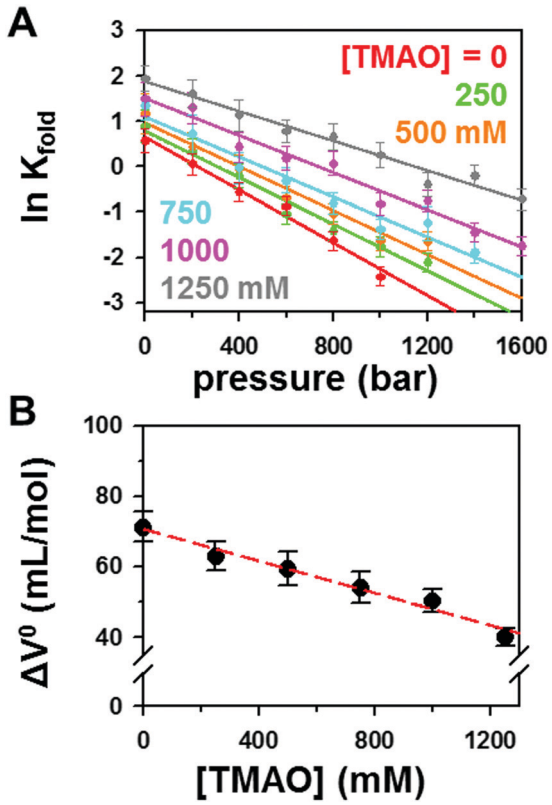

Fig. 8 Pressure dependence of folding at series of TMAO concentrations. (A) $\ln(K_{fold})$ *vs.* P plot where TMAO promotes folding and effectively reduces the slope (ΔV^0). (B) [TMAO] dependence of ΔV^0. ΔV^0 decrease linearly with [TMAO] concentration.

The pressure dependent data for $\ln(K_{fold})$ as a function of TMAO concentration are exhibited in Fig. 8A. We focus first on results at ambient pressure, $P \approx 1$ bar, for which the spread in intercepts indicates a moderate TMAO free energy enhancement in folding of the lysine riboswitch over the range of physiologically relevant concentrations sampled (0 mM to 1250 mM). This modest TMAO dependent (3–4 fold) increase in K_{fold} is consistent with previously characterized stabilization effects of TMAO osmolyte on nucleic acid structures.[39,68,69] However, it contrasts with the results obtained previously for lysine, Na^+ and Mg^{2+} cosolutes. This means that the free volume change for lysine riboswitch folding decreases significantly with TMAO osmolyte (see Fig. 8B and Table 3), indeed by nearly 50% by 1.25 M. Stated alternatively, this means that the lysine riboswitch unfolds much less effectively (*i.e.* is more stable) at higher [TMAO], with a difference in excess of 3–4 log units in $\ln(K_{fold})$ up at the highest pressures observed.

The results in Fig. 8A and B highlight two ways in which TMAO provides a protective mechanism against changes in external pressure, which could be crucially important in maintaining accessibility of marine species to wider range of vertical depth profiles. Firstly, the compaction of curves in Fig. 8A near ambient pressures indicates that TMAO increases folded lysine riboswitch stabilities only relatively modestly ($\approx$3–4 fold), which could be crucial to preserving biochemical function of the riboswitch.[35,67] This differs specifically from the more dramatic dependence of riboswitch stability on Mg^{2+}, which strongly favors riboswitch folding and thus completely switches the gene regulation on or off. Instead, TMAO at ambient pressures only shifts the equilibrium moderately toward the folded state. As a consequence, this allows the riboswitch to dynamically shift between two comparable free energy conformations and thereby still efficiently regulate gene expression.

As an important secondary effect, however, the incorporation of TMAO into the cell systematically decreases the slopes in Fig. 8A and thus creates an exponential sensitivity of K_{fold} on pressure. As a result, what are only modest riboswitch stabilization effects under low pressure ambient conditions grow exponentially stronger at higher pressure. More quantitatively, the slopes and intercepts in Fig. 8A indicate that [TMAO] = 1250 mM achieves an equivalent lysine riboswitch folding stability at $\sim$800 bar as obtained at ambient pressures in the complete absence of TMAO. This may signal an elegant strategy behind controlled build-up of osmolytes such as TMAO in cells. Specifically, it promotes biomolecular folding under high pressures and yet also maintains the requisite "on–off" two-state riboswitch sensitivity to lysine over a wider range of ocean depth profiles and external pressures.

Table 3 ΔV^0 obtained at increasing [TMAO]

[TMAO] (mM)	0	250	500	750	1000	1250
ΔV^0 (mL mol^{-1})	71(4)	63(4)	59(4)	54(4)	50(3)	40(2)

IV. Discussion

A. Pressure denaturation of lysine riboswitch folding

The pressure dependence of our biomolecular folding is dominated by the positive free volume difference between the folded and unfolded conformations ($\Delta V^0 = V^0_{fold} - V^0_{unfold} \approx +74$ mL mol^{-1}), which according to Le Chatelier's principle, predicts pressure-induced denaturation.[5] The physical reason why $\Delta V^0 > 0$ for the lysine riboswitch is not immediately obvious, since folded conformations of biopolymers are generally considered to be more compact. However, one must remember that measured ΔV^0 values represent changes for the entire solute + solvent system, for which the solvent can contribute significantly to the overall ΔV^0.[1–4] For instance, solvent voids can be generated due to formation of hydrophobic contacts upon folding, which can decrease the solvent accessible volume and result in a net outward displacement of the solvent ($\Delta V^0 > 0$).[2] Alternatively, the unfolded RNA conformation can expose the polyanionic backbone to more solvent (water) and thus can form a more compact hydration shell.[10,49] Since a more highly ordered hydration structure for the unfolded conformation takes up less volume,[10,49] this could translate into an increase in free volume ($\Delta V^0 > 0$) as the riboswitch folds and partially disrupts these water contacts. The potential for competition between solute *vs.* solvent volume changes makes unambiguous deconstruction of the contributions to ΔV^0 challenging.

However, it is the case that pressure-induced denaturation effects (which require $\Delta V^0 > 0$) have been noted in ensemble studies of many other protein and nucleic acid systems.[4,70]

Pressure-induced denaturation of the lysine riboswitch is clearly indicated in each of the $\ln(K_{fold})$ *vs.* pressure plots in Fig. 4–8, where negative slopes correspond to $\Delta V^0 > 0$ (eqn (1)). Interestingly, an increase in [lysine] stabilizes the folded conformation predominantly by parallel translation of the curves with negligible changes in the slope, consistent with $\Delta\Delta V^0 \approx 0$ (Fig. 4). What makes this particularly interesting is that it had been previously shown that the lysine riboswitch folding follows an ''induced-fit'' (bind-then-fold) mechanism and therefore its folded state is well characterized as ligand-bound.[28,29] This would imply that any [lysine] changes must therefore correlate with ligand binding to the unfolded conformation. As a result, the fact that $\Delta\Delta V^0$ with respect to lysine is experimentally small could reflect that the unfolded conformation is dominated by one of the two ligand-bound or ligand-free association states. This looks not to be the case, however, as a dissociation constant K_D = 1.7(5) mM for the unfolded conformation has been determined from previous single molecule kinetic studies.[28] which predicts both ligand-bound and ligand-free states to be significantly present at [lysine] $\approx$ 0.5–8 mM. Thus, the measured independence of ΔV^0 on [lysine] indicates the volumes of the ligand-bound and ligand-free unfolded states to be experimentally indistinguishable. It is also worth noting that the uncertainties in ΔV^0 are <5 mL mol^{-1}, *i.e.*, less than 1/3 the volume of a single water molecule.

From the pressure dependent folding data in Fig. 4, we obtain the apparent dissociation constant K_d for lysine and the corresponding 50% folding pressures ($P_{50\%}$) with which to characterize the pressure dependent riboswitch–ligand interaction. Since ΔV^0 is approximately independent of [lysine], K_d increases nearly exponentially with P (Fig. 5), clearly demonstrating that external pressure impedes cognate ligand-induced folding of the lysine riboswitch. This pressure-dependent binding constant for lysine decreases rapidly, with K_d predicted at the bottom of the Mariana Trench to be 3 orders of magnitude larger ($K_d \approx 300(60)$ mM) than at ambient pressures ($K_d \approx 0.31(10)$ mM). These results demonstrate that high pressure significantly disrupts the riboswitch–ligand interaction, which in deep sea species must therefore be compensated by some other protective mechanism (*e.g.*, osmotic enhancement) in order to maintain cellular function. Finally, we note that these smFRET burst fluorescence studies only report on the apparent dissociation constant K_d through observation of overall riboswitch folding. More specifically, we cannot rule out whether the increase in K_d occurs by a (i) pressure-dependent decrease in ligand affinity or (ii) pressure-dependent efficiency of the resulting ligand-promoted conformational change, although such questions should be addressed by single molecule kinetic studies on tethered constructs.

B. Cationic effects on the lysine riboswitch

The equilibrium for lysine riboswitch folding exhibits only a quite modest dependence on [Na^+] under both ambient and high-pressure conditions. Not only is the free volume change ΔV^0 effectively independent of [Na^+], but the riboswitch folding equilibrium constant (K_{fold}) is largely constant over the entire physiologically relevant range ([Na^+] = 100–250 mM). Since charge neutralization and Debye shielding is an essential prerequisite for RNA forming compact structures,[53,71] this is a bit surprising. Indeed, although monovalent cations are found to be less effective than divalent cations in stabilizing RNA tertiary structure, they are often still able to promote RNA folding at sufficiently high concentrations.[31,47,71] However, as discussed in Section IIIC, not all tertiary contacts in a full ribozyme can be effectively promoted by monovalent cations alone,[56,61–63] suggesting Mg^{2+} to be essential for RNA structure formation.[60] Moreover, these Na^+ dependent studies have been explored in the presence of [Mg^{2+}] = 0.5 mM in order to effectively promote the lysine binding.[28,44] It is unclear how Mg^{2+} competes with Na^+ to neutralize/solvate the RNA; thus the overall monovalent cation effects may still be dominated by Mg^{2+}, which is known to interact strongly with RNA.[65]

By way of contrast, Mg^{2+} is known to strongly promote RNA structure formation and has been shown in previous studies to be essential for lysine riboswitch folding,[23,28,44] primarily in promoting tertiary contacts and pre-organizing the ligand binding site.[45] It is thus not surprising that Mg^{2+} strongly stabilizes the folded lysine riboswitch, as evidenced by strong upward displacement of the semilogarithmic plots in Fig. 7A. Instead, it is the parallel nature of these curves as a function of Mg^{2+} (which implies an Mg^{2+}-independent change in ΔV^0) that becomes most noteworthy. Interestingly, although only a limited nucleic acid systems have been studied as a function of external pressure, ΔV^0 values for nucleic acid folding have been found to be small and [Mg^{2+}] sensitive.[22,57] For example, ΔV^0 for secondary structure formation in a DNA 40A hairpin is reduced from 11.5(35) mL mol^{-1} to 5.9(10) mL mol^{-1} between [Mg^{2+}] = 0.3–1.0 mM,[57] while ΔV^0 for folding of the tetraloop–receptor tertiary interaction motif is increased from 5(3)–9(2) mL mol^{-1} between [Mg^{2+}] = 0.0–1.0 mM.[22] As described in Section IIIC, such sign reversals in $\Delta\Delta V^0$ may result from preferential interaction of Mg^{2+} with folded *vs.* unfolded RNA conformations. This again provides additional motivation for high pressure kinetic studies at the single molecule level, which would permit further thermodynamic deconstruction of these equilibrium constants into forward (folding) and reverse (unfolding) rate constants over a transition state barrier.

Despite an RNA construct-dependent sign of $\Delta\Delta V^0$ with respect to divalent cation concentration, the data in Fig. 7A make clear that Mg^{2+} strongly stabilizes lysine riboswitch folding. In principle, this additional stabilization could also be used to protect lysine riboswitches from pressure-induced denaturation under deep sea conditions. However, the riboswitch gene regulatory mechanism relies on efficient, high dynamic range ''switching'' between on- and off-states of comparable free energy, triggered by presence or absence of the cognate ligand.[9] Therefore, overzealous stabilization of one of the two conformations by Mg^{2+} would shift this equilibrium and therefore be less desirable for robust riboswitch competency. This could represent yet another

reason why marine species do not accumulate divalent salts to modulate their cellular osmotic pressure, as these species could significantly perturb riboswitch equilibria and therefore biomolecular function.[35,67]

C. Osmolytic protection against pressure denaturation

As described in Section III and above, common monovalent (Na^+) and divalent (Mg^{2+}) cations exert a negligible influence on free volume changes ($\Delta\Delta V^0 \approx 0$) due to lysine riboswitch folding. As a result, modulation of cation concentrations should have little impact on riboswitch folding equilibria as a function of external pressure. Instead, marine species have evolved to accumulate small highly polar organic molecules ("osmolytes") to help achieve the correct osmotic balance between cellular and external environments.[32] Unlike inorganic cations, these osmolytes do not significantly alter biomolecular folding equilibria and may also protect the cell from multiple environmental stressors such as temperature and pressure.[67] Trimethylamine *N*-oxide (TMAO) is one of the most common of these osmolytes, empirically known to be crucial for survival of organisms at extreme deep sea pressures.[34] Indeed, TMAO concentrations in fish and amphipods increasing quasi linearly with ocean depth up to as high as [TMAO] $\approx$ 0.5 M.[34,35] TMAO has explicitly been shown to protect proteins and DNA helices from pressure-induced denaturation,[57,72] while effects on the stability of RNA tertiary folding under pressure have remained largely unexplored. Although the precise biological mechanism for protection against high external hydrostatic pressure in deep sea bacteria is still unclear, our current study of TMAO pressure-induced denaturation of the lysine riboswitch highlights some useful principles for identifying potential "piezolytes," which can hope to counteract external pressure effects by not only stabilizing biomolecular folding of the riboswitch but also reducing pressure sensitivity to riboswitch folding formation by control of $\Delta\Delta V^0$.

From pressure dependent plots of $\ln(K_{fold})$ *vs.* [TMAO] (see Fig. 8A), the folded lysine riboswitch is stabilized (*i.e.*, K_{fold} increases with [TMAO]) all the way down to ambient pressure (1 bar). There are three closely related predictions and corollaries from Fig. 8A that bear emphasizing, all arising from the simple observation in Fig. 8B of a negative $\Delta\Delta V^0$. (1) First and foremost is that the pressure dependence becomes weaker (*i.e.*, the slopes become shallower) with increasing [TMAO]. (2) The corollary is that increasing [TMAO] does not shift folding equilibria as dramatically at low *vs.* high pressure conditions. As a result, the concentration/pressure "phase space" over which $\ln(K_{fold}) \approx 0$ and thus riboswitch functionality is maximized, which can be argued is an essential characteristic of a good osmolyte. (3) The third implication is that the $\ln(K_{fold})$ plots naturally fan out with increasing P, and thus by control of TMAO levels, permit access to an exponentially larger dynamic range for osmolytic stabilization of the riboswitch under elevated pressure conditions. The combination of these three predictions, all fundamentally arising from $\Delta\Delta V^0 < 0$, therefore extends the biochemically functional range of the lysine riboswitch for gene regulation over a greater dynamic range of pressures.

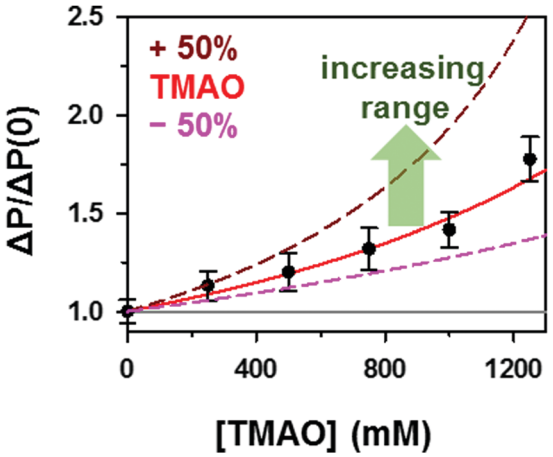

Fig. 9 Accessible pressure range for the lysine riboswitch as a function of [TMAO], normalized to the corresponding pressure range at [TMAO] = 0. The grey solid line corresponds the pressure range without osmolyte effects. The red solid line represents predictions from the fit of the [TMAO] dependence of ΔV^0 with m = −0.0228(18) mL mol^{-1} mM^{-1}. The dashed lines indicate effects due to the uncertainty in m on the pressure range as a function of [osmolyte]: 50% larger (dark red) and 50% smaller (pink) m values.

We attempt to capture this point in Fig. 9, based on the pressure range over which the lysine riboswitch properly functions. We can roughly estimate this range as $\Delta P = P_{max} - P_{min}$ whereby K_{fold} changes by some small factor κ, which based on elementary thermodynamics of reversible work ($P \approx \Delta(\Delta G^0)/\Delta V^0$), translates into $\Delta P \approx 2RT\ln(\kappa)/\Delta V^0$. Next, we least squares fit the [TMAO] dependence of $\Delta(\Delta V^0)$ in Fig. 8B to a simple linear function $\Delta V^0(0) + m$[osmolyte] ($\Delta V^0(0)$ = 70.6(13) mL mol^{-1}, slope m = −0.0228(18) mL mol^{-1} mM^{-1}). The explicit influence of TMAO on pressure dependent folding can therefore be plotted as ΔP for finite [TMAO] normalized to $\Delta P(0)$ at [TMAO] = 0, which from Fig. 9 can be seen to increase nearly 70% over [TMAO] = 0.00–1.25 M. Finally, it is worth noting that this normalization process yields results conveniently independent of the arbitrary choice of κ. The results, however, do indicate the correct sensitivity to the experimentally fitted slopes, which predict an enhanced pressure range ($\Delta P/\Delta P(0) > 1$) for negative values of m. The sensitivity of the pressure range to the osmolyte effects (m) is also illustrated in Fig. 9 with dark red and pink curves corresponding to +50% and −50% m value of TMAO.

Since the environmental factors such as temperature, salinity and dissolved oxygen remain largely constant under deep sea conditions,[73] pressure represents the major limitation for deep sea organisms to migrate and survive at different depths. The data allow us to put this simple model on a more rigorous mathematical footing. For example, we can determine from Fig. 8A the 50% pressure ($P_{50\%}$) at each [TMAO] for an experimentally convenient value of the apparent dissociation constant (*e.g.*, at $K_{fold} \approx 1$, for which $K_d \approx$ [lysine] $\approx$ 0.5 mM). We can then use $\Delta G^0(P) = \Delta G^0(P=0) + P\Delta V^0 = -RT\ln(K_{fold}) \approx 0$ to plot in Fig. 10 a constant K_d ("iso-K_d") curve of accessible deep sea ocean pressures ($P \approx -\Delta G^0(P=0)/\Delta V^0$), which reveals a dramatic exponential increase in the accessible pressure range with increasing [TMAO]. Specifically, Fig. 10 makes clear that a

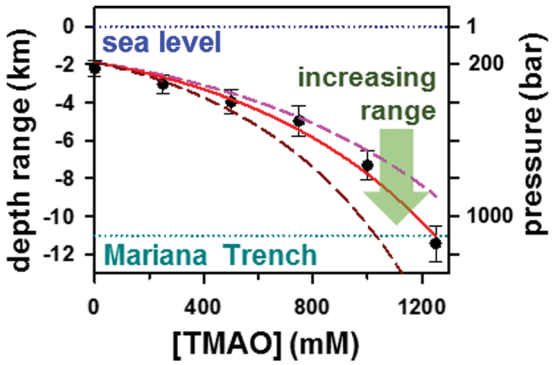

Fig. 10 Iso-K_d curve as a function of both pressure (depth in the ocean) and [TMAO] where K_d = 0.5 mM. K_d is maintained by [TMAO] = 1250 mM with Δ(ocean depth) > 9 km. Data fit to a negative exponential growth function (red), indicating the TMAO effects are even stronger at high concentrations. The dashed lines indicate the effects of changes in slope magnitude on the iso-K_d curve: +50% (dark red) and −50% (pink).

constant riboswitch–ligand affinity (K_d = 0.5 mM) can be maintained over a 900 bar pressure increase (≈9000 m vertical migration) by control of TMAO cellular concentrations between 0–1.25 M, with the TMAO stabilization effects becoming exponentially more significant at higher pressures. As a result, the sensitivity to the negative slope (m) is quite high, with the results for m and ±50% of m indicated as dashed lines in Fig. 10.

It is worth noting that the maximum [TMAO] values in this study are close to the theoretical upper bound of osmolyte concentration (~1.2 M, sea water) for marine species which tend to achieve either isosmotic or hypoosmotic conditions. Thus, the actual [TMAO] must in fact be lower due to additional salts, metabolites and other osmolytes required for cellular function. Our results therefore support the previous hypothesis[34] that fish may be constrained from inhabiting the deepest part of the sea below ~8500 m due to these limits on TMAO (~0.5 M). However, despite this crucial role in promoting biomolecule stability, the fact that fish are found at ~7000 m with only 0.5 M TMAO indicates [TMAO] can not be the sole factor for deep sea species to survive high pressures. Indeed, genetic adaptation for deep sea organisms can facilitate utilization of more pressure resistant protein and nucleic acid structures[40] as well as synergies between TMAO and other osmolytes/cosolutes to increase biomolecular stability. One important example would be that of "macromolecular crowding," which can not only stabilize biomolecule structures but also increase the effective concentration/activity of TMAO by taking up intracellular space.[11]

As a final comment, we can attempt a linear deconstruction of these free volume changes (ΔV^0) into solvent voids (ΔV^0_{void}) plus solvent hydration effects ($\Delta V^0_{hydration}$).[1,3,18] The relatively constant values of E_{FRET} values that we observe as a function of [TMAO] supports that TMAO does not significantly change the lysine riboswitch conformation nor the overall compactness of the folded state. This in turn suggests that $\Delta V^0_{void} \approx$ constant, from which the linear dependence of ln(K_{fold}) on [TMAO] in Fig. 8B could be entirely ascribed to hydration contributions ($\Delta V^0_{hydration}$) linearly proportional to [TMAO]. Indeed, TMAO has been found in previous studies to be excluded from the surfaces of proteins and RNA tertiary folding motifs[74–76] and also to greatly enhance the water structure,[77] thereby reducing the effective volume of the bulk water.[10,49] It is likely that since TMAO tend to orient the water molecules in the bulk, it reduces the effective volume difference between water molecules in the solvation shell of RNA and in the bulk, and consequently mitigate the pressure effects by reducing $\Delta V^0_{hydration}$. The linear decrease of ΔV^0 (Fig. 8B) which expands a wide range of [TMAO] can be simply explained by the fact that TMAO primarily affects the bulk water instead of the hydration shell surrounding the RNA.[76] Indeed, it has been found in previous molecular dynamics simulations that one hydrated TMAO is in close contact with 25 water molecules,[77] suggesting the bulk water (55.5 M) could be sufficiently ordered by the saturation [TMAO] at ~2.2 M. The dynamic range explored in this study for [TMAO] is still far from this saturation limit and thus might expect a linear decrease in ΔV^0 with increasing [TMAO]. It is also worth noting that since TMAO tends to remain strongly hydrated in the bulk water and interact only indirectly with RNA/protein,[74–76] the sign of these TMAO effects ($\Delta\Delta V^0 < 0$) is likely to be more universal and system-independent, making it an ideal piezolyte with which to protect biomolecular structures from pressure-induced denaturation.

V. Summary and conclusion

The pressure dependence of lysine riboswitch folding has been investigated at the single molecule level with smFRET spectroscopy and up to $P \approx 1500$ bar pressures. The lysine riboswitch unfolds readily at increasing pressure, with a change in free volume determined from linear pressure van't Hoff plots to be $\Delta V^0 = V_{fold} - V_{unfold} \approx 75(3)$ mL mol^{-1}. These data can be replotted as an apparent lysine riboswitch dissociation constant K_d as a function of P, which reveals the riboswitch–ligand interaction to be weakened quasi-exponentially with increasing pressure. While monovalent Na^+ effects on the free volume change are found to be negligible, the presence of divalent Mg^{2+} greatly stabilizes the folded lysine riboswitch at all pressures, with only negligible changes in ΔV^0 for both Mg^{2+} and Na^+ cations. By way of contrast, TMAO, a known piezolyte, is found to increase pressure stability of the riboswitch by simultaneously promoting folding (increase in K_{fold}) and reducing the folding-induced change in free volume ($\Delta\Delta V^0 < 0$). We argue that the latter influence of TMAO on free volume can play a crucial role in migration of deep sea species to different ocean depth layers of water in search of sparse resources. Moreover, we introduce an empirical deconstruction of the overall free volume change (ΔV^0) into solvent void formation (ΔV^0_{void}) and changes in the hydration layer ($\Delta V^0_{hydration}$) upon folding. The insensitivity of observed E_{FRET} values suggests that TMAO does not significantly alter the folded riboswitch conformation and thus that ΔV^0_{void} remains approximately constant over a variety of osmolyte conditions. If this is true, our deconstruction would identify the sign of $\Delta V^0 > 0$ to be due to changes in hydration effects.

Furthermore, since TMAO is known to be excluded from biomolecular surfaces and to enhance the formation of ordered water, this would be consistent with a linear reduction in ΔV^0 by TMAO over a wide range of concentration due to greater ordering of the bulk water structure and thereby lesser importance of RNA hydration effects.

Conflicts of interest

There are no conflicts to declare.

Acknowledgements

Initial funding for this work has been provided by the National Science Foundation (CHE-1665271, PHY 1734006) with ongoing support from the Air Force Office of Scientific Research (FA9550-15-1-0090). We would also like to acknowledge early contributions by the W. M. Keck Foundation Initiative in RNA Sciences at the University of Colorado, Boulder.

References

1 T. V. Chalikian and K. J. Breslauer, On Volume Changes Accompanying Conformational Transitions of Biopolymers, *Biopolymers*, 1996, **39**, 619–626.
2 J. Roche, J. A. Caro, D. R. Norberto, P. Barthe, C. Roumestand, J. L. Schlessman, A. E. Garcia, E. B. García-Moreno and C. A. Royer, Cavities Determine the Pressure Unfolding of Proteins, *Proc. Natl. Acad. Sci. U. S. A.*, 2012, **109**, 6945–6950.
3 N. V. Nucci, B. Fuglestad, E. A. Athanasoula and A. J. Wand, Role of Cavities and Hydration in the Pressure Unfolding of T_4 Lysozyme, *Proc. Natl. Acad. Sci. U. S. A.*, 2014, **111**, 13846–13851.
4 J. Roche and A. Royer Catherine, Lessons from Pressure Denaturation of Proteins, *J. R. Soc., Interface*, 2018, **15**, 20180244.
5 V. V. Mozhaev, K. Heremans, J. Frank, P. Masson and C. Balny, High Pressure Effects on Protein Structure and Function, *Proteins*, 1996, **24**, 81–91.
6 F. Meersman, I. Daniel, D. H. Bartlett, R. Winter, R. Hazael and P. F. McMillan, High-Pressure Biochemistry and Biophysics, *Rev. Mineral. Geochem.*, 2013, **75**, 607–648.
7 E. Epping, Life in an Oceanic Extreme, *Nat. Geosci.*, 2013, **6**, 252–253.
8 A. S. Mironov, I. Gusarov, R. Rafikov, L. E. Lopez, K. Shatalin, R. A. Kreneva, D. A. Perumov and E. Nudler, Sensing Small Molecules by Nascent RNA: A Mechanism to Control Transcription in Bacteria, *Cell*, 2002, **111**, 747–756.
9 A. D. Garst, A. L. Edwards and R. T. Batey, Riboswitches: Structures and Mechanisms, *Cold Spring Harbor Perspect. Biol.*, 2011, **3**, a003533.
10 J. F. Lemay, J. C. Penedo, R. Tremblay, D. M. Lilley and D. A. Lafontaine, Folding of the Adenine Riboswitch, *Chem. Biol.*, 2006, **13**, 857–868.
11 K. T. Schroeder, P. Daldrop and D. M. Lilley, RNA Tertiary Interactions in a Riboswitch Stabilize the Structure of a Kink Turn, *Structure*, 2011, **19**, 1233–1240.
12 H. L. Sung and D. J. Nesbitt, DNA Hairpin Hybridization under Extreme Pressures: A Single-Molecule Fret Study, *J. Phys. Chem. B*, 2020, **124**, 110–120.
13 J. Q. Wu and R. B. Macgregor Jr., Pressure Dependence of the Helix–Coil Transition Temperature of Poly[D(G-C)], *Biopolymers*, 1995, **35**, 369–376.
14 R. Najaf-Zadeh, J. Q. Wu and R. B. Macgregor, Effect of Cations on the Volume of the Helix-Coil Transition of Poly[D(a-T)], *Biochim. Biophys. Acta, Gene Struct. Expression*, 1995, **1262**, 52–58.
15 G. Rayan and R. B. Macgregor, Pressure-Induced Helix–Coil Transition of DNA Copolymers Is Linked to Water Activity, *Biophys. Chem.*, 2009, **144**, 62–66.
16 G. Rayan, R. B. Macgregor and A. Look, at the Effect of Sequence Complexity on Pressure Destabilisation of DNA Polymers, *Biophys. Chem.*, 2015, **199**, 34–38.
17 S. Patra, C. Anders, N. Erwin and R. Winter, Osmolyte Effects on the Conformational Dynamics of a DNA Hairpin at Ambient and Extreme Environmental Conditions, *Angew. Chem., Int. Ed.*, 2017, **56**, 5045–5049.
18 S. Patra, C. Anders, P. H. Schummel and R. Winter, Antagonistic Effects of Natural Osmolyte Mixtures and Hydrostatic Pressure on the Conformational Dynamics of a DNA Hairpin Probed at the Single-Molecule Level, *Phys. Chem. Chem. Phys.*, 2018, **20**, 13159–13170.
19 H. Y. Fan, Y. L. Shek, A. Amiri, D. N. Dubins, H. Heerklotz, R. B. Macgregor and T. V. Chalikian, Volumetric Characterization of Sodium-Induced G-Quadruplex Formation, *J. Am. Chem. Soc.*, 2011, **133**, 4518–4526.
20 S. Takahashi and N. Sugimoto, Effect of Pressure on Thermal Stability of G-Quadruplex DNA and Double-Stranded DNA Structures, *Molecules*, 2013, **18**, 13297–13319.
21 L. Arns, J.-M. Knop, S. Patra, C. Anders and R. Winter, Single-Molecule Insights into the Temperature and Pressure Dependent Conformational Dynamics of Nucleic Acids in the Presence of Crowders and Osmolytes, *Biophys. Chem.*, 2019, **251**, 106190.
22 C. D. Downey, R. L. Crisman, T. W. Randolph and A. Pardi, Influence of Hydrostatic Pressure and Cosolutes on RNA Tertiary Structure, *J. Am. Chem. Soc.*, 2007, **129**, 9290–9291.
23 A. D. Garst, A. Héroux, R. P. Rambo and R. T. Batey, Crystal Structure of the Lysine Riboswitch Regulatory mRNA Element, *J. Biol. Chem.*, 2008, **283**, 22347–22351.
24 S. Schneider, H. Paulsen, K. C. Reiter, E. Hinze, C. Schiene-Fischer and C. G. Hübner, Single Molecule Fret Investigation of Pressure-Driven Unfolding of Cold Shock Protein A, *J. Chem. Phys.*, 2018, **148**, 123336.
25 A. Ben-Naim, Solvent Effects on Protein Association and Protein Folding, *Biopolymers*, 1990, **29**, 567–596.
26 P. J. Mikulecky and A. L. Feig, Heat Capacity Changes in RNA Folding: Application of Perturbation Theory to Hammerhead Ribozyme Cold Denaturation, *Nucleic Acids Res.*, 2004, **32**, 3967–3976.

27 H.-L. Sung and D. J. Nesbitt, Novel Heat-Promoted Folding Dynamics of the Yybp-Ykoy Manganese Riboswitch: Kinetic and Thermodynamic Studies at the Single-Molecule Level, *J. Phys. Chem. B*, 2019, **123**, 5412–5422.
28 L. R. Fiegland, A. D. Garst, R. T. Batey and D. J. Nesbitt, Single-Molecule Studies of the Lysine Riboswitch Reveal Effector-Dependent Conformational Dynamics of the Aptamer Domain, *Biochemistry*, 2012, **51**, 9223–9233.
29 H.-L. Sung and D. J. Nesbitt, Single-Molecule Fret Kinetics of the Mn^{2+} Riboswitch: Evidence for Allosteric Mg^{2+} Control of ''Induced-Fit'' Vs ''Conformational Selection'' Folding Pathways, *J. Phys. Chem. B*, 2019, **123**, 2005–2015.
30 Z.-J. Tan and S.-J. Chen, Nucleic Acid Helix Stability: Effects of Salt Concentration, Cation Valence and Size, and Chain Length, *Biophys. J.*, 2006, **90**, 1175–1190.
31 J. L. Fiore, E. D. Holmstrom, L. R. Fiegland, J. H. Hodak and D. J. Nesbitt, The Role of Counterion Valence and Size in GAAA Tetraloop–Receptor Docking/Undocking Kinetics, *J. Mol. Biol.*, 2012, **423**, 198–216.
32 P. Yancey, M. Clark, S. Hand, R. Bowlus and G. Somero, Living with Water Stress: Evolution of Osmolyte Systems, *Science*, 1982, **217**, 1214–1222.
33 P. H. Yancey, W. R. Blake and J. Conley, Unusual Organic Osmolytes in Deep-Sea Animals: Adaptations to Hydrostatic Pressure and Other Perturbants, *Comp. Biochem. Physiol., Part A: Mol. Integr. Physiol.*, 2002, **133**, 667–676.
34 P. H. Yancey, M. E. Gerringer, J. C. Drazen, A. A. Rowden and A. Jamieson, Marine Fish May Be Biochemically Constrained from Inhabiting the Deepest Ocean Depths, *Proc. Natl. Acad. Sci. U. S. A.*, 2014, **111**, 4461–4465.
35 A. B. Downing, G. T. Wallace and P. H. Yancey, Organic Osmolytes of Amphipods from Littoral to Hadal Zones: Increases with Depth in Trimethylamine N-Oxide, Scyllo-Inositol and Other Potential Pressure Counteractants, *Deep-Sea Res.*, 2018, **138**, 1–10.
36 B. J. Bennion and V. Daggett, Counteraction of Urea-Induced Protein Denaturation by Trimethylamine N-Oxide: A Chemical Chaperone at Atomic Resolution, *Proc. Natl. Acad. Sci. U. S. A.*, 2004, **101**, 6433–6438.
37 C. A. Royer, Revisiting Volume Changes in Pressure-Induced Protein Unfolding, *Biochim. Biophys. Acta, Protein Struct. Mol. Enzymol.*, 2002, **1595**, 201–209.
38 G. N. Somero, Biochemical Ecology of Deep-Sea Animals, *Experientia*, 1992, **48**, 537–543.
39 E. D. Holmstrom, N. F. Dupuis and D. J. Nesbitt, Kinetic and Thermodynamic Origins of Osmolyte-Influenced Nucleic Acid Folding, *J. Phys. Chem. B*, 2015, **119**, 3687–3696.
40 T. Morita, Structure-Based Analysis of High Pressure Adaptation of A-Actin, *J. Biol. Chem.*, 2003, **278**, 28060–28066.
41 J.-B. Rouget, T. Aksel, J. Roche, J.-L. Saldana, A. E. Garcia, D. Barrick and C. A. Royer, Size and Sequence and the Volume Change of Protein Folding, *J. Am. Chem. Soc.*, 2011, **133**, 6020–6027.
42 P. H. Yancey, A. L. Fyfe-Johnson, R. H. Kelly, V. P. Walker and M. T. Auñón, Trimethylamine Oxide Counteracts Effects of Hydrostatic Pressure on Proteins of Deep-Sea Teleosts, *J. Exp. Zool.*, 2001, **289**, 172–176.
43 A. Sengupta, H.-L. Sung and D. J. Nesbitt, Amino Acid Specific Effects on RNA Tertiary Interactions: Single-Molecule Kinetic and Thermodynamic Studies, *J. Phys. Chem. B*, 2016, **120**, 10615–10627.
44 S. Blouin, R. Chinnappan and D. A. Lafontaine, Folding of the Lysine Riboswitch: Importance of Peripheral Elements for Transcriptional Regulation, *Nucleic Acids Res.*, 2010, **39**, 3373–3387.
45 K. McCluskey, J. Boudreault, P. St-Pierre, C. Perez-Gonzalez, A. Chauvier, A. Rizzi, P. B. Beauregard, D. A. Lafontaine and J. C. Penedo, Unprecedented Tunability of Riboswitch Structure and Regulatory Function by Sub-Millimolar Variations in Physiological Mg^{2+}, *Nucleic Acids Res.*, 2019, **47**, 6478–6487.
46 M. Vieweger, E. D. Holmstrom and D. J. Nesbitt, Single-Molecule Fret Reveals Three Conformations for the TLS Domain of Brome Mosaic Virus Genome, *Biophys. J.*, 2015, **109**, 2625–2636.
47 J. L. Fiore, J. H. Hodak, O. Piestert, C. D. Downey and D. J. Nesbitt, Monovalent and Divalent Promoted GAAA Tetraloop–Receptor Tertiary Interactions from Freely Diffusing Single-Molecule Studies, *Biophys. J.*, 2008, **95**, 3892–3905.
48 J. L. Fiore, B. Kraemer, F. Koberling, R. Edmann and D. J. Nesbitt, Enthalpy-Driven RNA Folding: Single-Molecule Thermodynamics of Tetraloop−Receptor Tertiary Interaction, *Biochemistry*, 2009, **48**, 2550–2558.
49 F. Merzel and J. C. Smith, Is the First Hydration Shell of Lysozyme of Higher Density Than Bulk Water?, *Proc. Natl. Acad. Sci. U. S. A.*, 2002, **99**, 5378–5383.
50 D. A. Nicholson, A. Sengupta, H.-L. Sung and D. J. Nesbitt, Amino Acid Stabilization of Nucleic Acid Secondary Structure: Kinetic Insights from Single-Molecule Studies, *J. Phys. Chem. B*, 2018, **122**, 9869–9876.
51 K. Furukawa, H. Gu, N. Sudarsan, Y. Hayakawa, M. Hyodo and R. R. Breaker, Identification of Ligand Analogues That Control C-Di-Gmp Riboswitches, ACS, *Chem. Biol.*, 2012, **7**, 1436–1443.
52 J. C. Bowman, T. K. Lenz, N. V. Hud and L. D. Williams, Cations in Charge: Magnesium Ions in RNA Folding and Catalysis, *Curr. Opin. Struct. Biol.*, 2012, **22**, 262–272.
53 J. Liu, A. C. Declais, S. A. McKinney, T. Ha, D. G. Norman and D. M. J. Lilley, Stereospecific Effects Determine the Structure of a Four-Way DNA Junction, *Chem. Biol.*, 2005, **12**, 217–228.
54 S. A. McKinney, A. D. Freeman, D. M. J. Lilley and T. Ha, The Rugged Energy Landscape of Holliday Junction Branch Migration and Its Impact on Resolution, *Biophys. J.*, 2005, **88**, 14A.
55 T. J. Wilson, M. Nahas, L. Araki, S. Harusawa, T. Ha and D. M. J. Lilley, RNA Folding and the Origins of Catalytic Activity in the Hairpin Ribozyme, *Blood Cells, Mol., Dis.*, 2007, **38**, 8–14.
56 I. Shcherbakova, S. Gupta, M. R. Chance and M. Brenowitz, Monovalent Ion-Mediated Folding of the Tetrahymena Thermophila Ribozyme, *J. Mol. Biol.*, 2004, **342**, 1431–1442.

57 S. Patra, V. Schuabb, I. Kiesel, J.-M. Knop, R. Oliva and R. Winter, Exploring the Effects of Cosolutes and Crowding on the Volumetric and Kinetic Profile of the Conformational Dynamics of a Poly Da Loop DNA Hairpin: A Single-Molecule Fret Study, *Nucleic Acids Res.*, 2018, **47**, 981–996.
58 M. K. Nahas, T. J. Wilson, S. C. Hohng, K. Jarvie, D. M. J. Lilley and T. Ha, Observation of Internal Cleavage and Ligation Reactions of a Ribozyme, *Nat. Struct. Mol. Biol.*, 2004, **11**, 1107–1113.
59 A. Iqbal, L. Wang, K. C. Thompson, D. M. J. Lilley and D. G. Norman, The Structure of Cyanine 5 Terminally Attached to Double-Stranded DNA: Implications for Fret Studies, *Biochemistry*, 2008, **47**, 7857–7862.
60 C. Joo, S. A. McKinney, D. M. J. Lilley and T. Ha, Exploring Rare Conformational Species and Ionic Effects in DNA Holliday Junctions Using Single-Molecule Spectroscopy, *J. Mol. Biol.*, 2004, **341**, 739–751.
61 T. J. Wilson, M. Nahas, T. Ha and D. M. J. Lilley, Folding and Catalysis of the Hairpin Ribozyme, *Biochem. Soc. Trans.*, 2005, **33**, 461–465.
62 S. Hohng, T. J. Wilson, E. Tan, R. M. Clegg, D. M. J. Lilley and T. Ha, Conformational Flexibility of Four-Way Junctions in RNA, *J. Mol. Biol.*, 2004, **336**, 69–79.
63 T. A. Goody, S. E. Melcher, D. G. Norman and D. M. J. Lilley, The Kink-Turn Motif in RNA Is Dimorphic, and Metal Ion-Dependent, *RNA*, 2004, **10**, 254–264.
64 L. Huang and D. M. J. Lilley, The Kink Turn, a Key Architectural Element in RNA Structure, *J. Mol. Biol.*, 2016, **428**, 790–801.
65 M. Nahas, T. J. Wilson, S. C. Hohng, K. Jarvie, D. M. J. Lilley and T. Ha, Observation of Internal Cleavage and Ligation Reactions of a Ribozyme (vol. 11, p. 1107, 2004), *Nat. Struct. Mol. Biol.*, 2004, **11**, 1253.
66 R. Forster and L. Goldstein, Intracellular Osmoregulatory Role of Amino Acids and Urea in Marine Elasmobranchs, *Am. J. Physiol.*, 1976, **230**, 925–931.
67 P. H. Yancey, Organic Osmolytes as Compatible, Metabolic and Counteracting Cytoprotectants in High Osmolarity and Other Stresses, *J. Exp. Biol.*, 2005, **208**, 2819–2830.
68 T. C. Gluick and S. Yadav, Trimethylamine N-Oxide Stabilizes RNA Tertiary Structure and Attenuates the Denaturating Effects of Urea, *J. Am. Chem. Soc.*, 2003, **125**, 4418–4419.
69 D. Lambert and D. E. Draper, Effects of Osmolytes on RNA Secondary and Tertiary Structure Stabilities and RNA-Mg2+ Interactions, *J. Mol. Biol.*, 2007, **370**, 993–1005.
70 R. B. Macgregor Jr., Effect of Hydrostatic Pressure on Nucleic Acids, *Biopolymers*, 1998, **48**, 253–263.
71 B. Okumus, T. J. Wilson, D. M. J. Lilley and T. Ha, Vesicle Encapsulation Studies Reveal That Single Molecule Ribozyme Heterogeneities Are Intrinsic, *Biophys. J.*, 2004, **87**, 2798–2806.
72 C. Krywka, C. Sternemann, M. Paulus, M. Tolan, C. Royer and R. Winter, Effect of Osmolytes on Pressure-Induced Unfolding of Proteins: A High-Pressure SAXS Study, *ChemPhysChem*, 2008, **9**, 2809–2815.
73 E. Tan, T. J. Wilson, M. K. Nahas, R. M. Clegg, D. M. J. Lilley and T. Ha, A Four-Way Junction Accelerates Hairpin Ribozyme Folding Via a Discrete Intermediate, *Proc. Natl. Acad. Sci. U. S. A.*, 2003, **100**, 9308–9313.
74 D. R. Canchi, P. Jayasimha, D. C. Rau, G. I. Makhatadze and A. E. Garcia, Molecular Mechanism for the Preferential Exclusion of TMAO from Protein Surfaces, *J. Phys. Chem. B*, 2012, **116**, 12095–12104.
75 D. M. J. Lilley, Structure, Folding and Mechanisms of Ribozymes, *Curr. Opin. Struct. Biol.*, 2005, **15**, 313–323.
76 D. A. Lafontaine, D. G. Norman and D. M. Lilley, Structure, Folding and Activity of the VS Ribozyme: Importance of the 2-3-6 Helical Junction, *EMBO J.*, 2001, **20**, 1415–1424.
77 S. A. McKinney, E. Tan, T. J. Wilson, M. K. Nahas, A. C. Declais, R. M. Clegg, D. M. J. Lilley and T. Ha, Single-Molecule Studies of DNA and RNA Four-Way Junctions, *Biochem. Soc. Trans.*, 2004, **32**, 41–45.

